SCIENTIFIC REPORTS

OPEN

Martensitic transformation of $Ti_{50}(Ni_{50-x}Cu_x)$ and $Ni_{50}(Ti_{50-x}Zr_x)$ shape-memory alloys

Received: 11 July 2018
Accepted: 8 February 2019
Published online: 01 March 2019

Xiaolan Yang[1,2], Lei Ma[1] & Jiaxiang Shang[1]

Martensitic transformation and phase stability of $Ti_{50}(Ni_{50-x}Cu_x)$ and $Ni_{50}(Ti_{50-x}Zr_x)$ shape memory alloys are investigated based on density functional theory (DFT). According to the results of formation energy we calculated, upon substitution of Ni by Cu at levels of about 10.4 at.%, $Ti_{50}(Ni_{50-x}Cu_x)$ alloys lose the monoclinic martensite in favor of the orthorhombic martensite structure. The martensite monoclinic B19′ structure of $Ni_{50}(Ti_{50-x}Zr_x)$ becomes more stable with increasing of the Zr content. The energy difference between austenite and martensite decreases when Cu < 10.4 at.%, and then increases slightly, which suggesting that Cu addition reduces the composition sensitivity of martensitic transformation temperature comparing with binary NiTi alloys. The energy difference decreases slightly firstly when Zr < 10.4 at.% and then increases sharply, which indicates that Zr addition increases martensitic transformation temperature dramatically. Furthermore, a geometric model is used to evaluate the thermal hysteresis. More interestingly, it is found that the lowest thermal hysteresis is achieved at 10.4 at.% for Cu-doped NiTi; whereas the thermal hysteresis increases with increasing of Zr. The electronic structures of austenite phase are also discussed in detail.

Among the reported shape memory alloys (SMAs), NiTi alloys are the most attractive ones due to their unique shape memory effect and excellent superelasticity, resulting from the reversible thermoelastic martensite transformation (MT) between the high-temperature austenite phase and low-temperature martensite phases[1]. NiTi SMAs have been studied extensively and widely used for a variety of applications in a number of different fields, such as aeronautic, microelectronic and biomedical industries, since 1960s when first discovered by Buehler and Wiley[2]. However, some applications of the NiTi SMAs are greatly limited by its particular hysteresis (ΔT) and the martensite transformation temperature, T_m, is usually lower than 100 °C[3]. The need of addressing these limitations has led to numerous experimental and theoretical researches[4–15].

The addition of Fe and Co (substituted for Ni) or Al, V, Cr and Mn (substituted for Ti)[4] depresses the T_m of NiTi alloys severely even at very small levels, but still results in a monoclinic martensite phase after MT. According to the recent reports[5,6], there exists a strain glass (STG) transition in doped $Ti_{50}(Ni_{50-x}D_x)$ (D = Co, Cr, Mn) alloys. Wang *et al.*[7] discovered the existence of strain glass in $Ti_{50}Ni_{50-x}Fe_x$, beyond a critical Fe doping level $x > x_c$ ($5 < x_c < 6$). Alloying NiTi with Cu (Cu substitutes for Ni) reduces the thermal hysteresis[8] and composition sensitivity of the transformation temperatures[9], meanwhile, changes the MT pathway[8,16,17].

Transformation temperature increases linearly with the X content for alloys containing greater than approximately 10–15 at.% in ternary NiTi-X (X = Zr, Hf, Pd and Pt) SMAs[10]. These high-temperature shape memory alloys (HTSMAs) with the T_m higher than 100 °C have various potential applications. NiTiZr system has drawn much attention owing to the much lower cost compared with the noble metals (Pd, Pt, and Au). Experiments have indicated that, the T_m decreases with small amounts of Zr ($X \leq 3$ at.%)[18], and then sharply increases when Zr content exceeds 10 at.%, approaches as high as 170 °C for 20.2 at.% Zr[11–13]; martensite structure remains monoclinic (B19′)[11,12]; and its hysteresis is slightly wider than that of TiNi binary alloy[13]. Frenzel *et al.*[19] found the strong dependence of T_m on alloy composition in binary NiTi, ternary Ni–Ti–X (X = Cr, Cu, Hf, Pd, V, Zr) and quaternary Ni–Ti–Cu–Y (Y = Co, Pd) SMAs.

From above experimental researches, it can be seen that the alloying elements play an important role in determining the phase transformation temperature, hysteresis as well as STG. Zarinejad and Liu[20] conclude that the valence electron concentration is found to be an important parameter influencing the T_m. There requires a better

[1]School of Materials Science and Engineering, Beihang University, Beijing, 100191, China. [2]School of Physics and Electronic Science, Zunyi Normal College, Zunyi, 563002, China. Correspondence and requests for materials should be addressed to J.S. (email: shangjx@buaa.edu.cn)

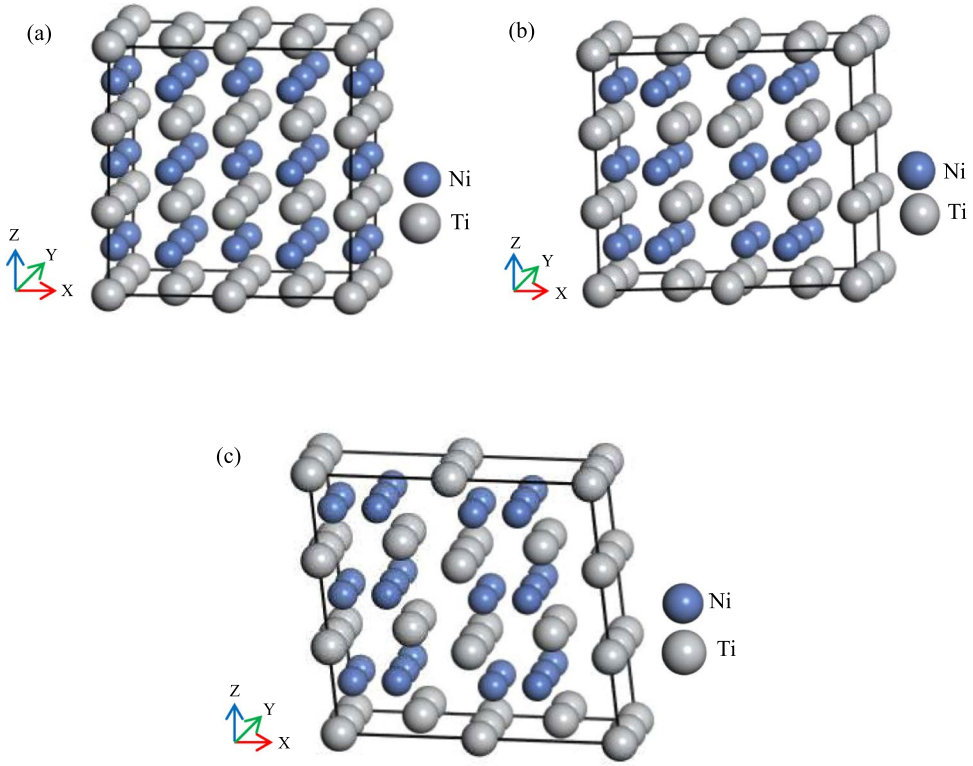

Figure 1. Schematic diagram of the $2 \times 2 \times 3$ supercell model of austenite and martensite phase of NiTi alloy: (**a**) B2, (**b**) B19 and (**c**) B19′. Smaller blue spheres are Ni atoms; larger gray spheres are Ti atoms.

understanding of how they affect the phase structure and properties and the strong composition dependence of T_m.

The first-principles has been used to study the microscopic origin of NiTi MT further. Recently, the site preference for ternary additions in NiTi has been systematic calculated[21]. The martensite crystal structures of $Ti_{50}Ni_{50-x}Cu_x$ SMAs were investigated by using CASTEP code[22]. Wang's ab-initio calculations[6] show the origin of STG transition in $Ti_{50}(Ni_{50-x}D_x)$ (D = Cr, Mn, Fe and Co) alloys, and indicate that Cu and Pd cannot induce the STG transition. Hu *et al.*[14] investigated the alloying effect of Zr on the elastic properties of Ni-rich Ni–Ti–Zr HTSMAs. Our previous work[15] has investigated the effect of Pd on the martensitic transformation of Ni–Ti–Pd HTSMAs through DFT calculations. Attracted by the small hysteresis width[8] and the low composition sensitivity of T_m[9] in Ni–Ti–Cu alloys, the relatively low materials cost and large change of T_m in Ni–Ti–Zr HTSMAs[10–13]. Consequently, we devote this paper to study the phase stability and transition behaviors of Ni–Ti–Cu and Ni–Ti–Zr alloys based on DFT, further rationalize the experimental findings about MT, and explain the strong content dependence of the phase stability of martensite crystal structure, transformation temperature and thermal hysteresis.

Generally, the DFT calculations are implemented at the temperature of 0 K[23]. As we are just concerned with the relative variations of the energy between austenite and martensite phases, the energy differences are almost unaffected by temperature. Transmission electron microscopy shows the presence of precipitates in Ni–Ti–Cu films after aging, precipitations vary with different annealings[24]. The effect of precipitation is beyond of the scope of the current work.

Computational Models and Methods

We focus only on the Ti-deficient Ni–Ti–Zr and Ni-deficient Ni–Ti–Cu alloys[4], thus antisite defects were not discussed in the present work. In this paper, we adopt the $Ti_{50}(Ni_{50-x}Cu_x)$ and $Ni_{50}(Ti_{50-x}Zr_x)$ ($x = 4.2$, 6.3, 8.4, 10.4, 12.5, 18.8, 25) alloys as our modeling. Considering the symmetry of the cell, a $2 \times 2 \times 3$ supercell containing 48 atoms of the austenite phase is chosen, and X, Y, Z directions are along $[001]_{B2}$, $[\bar{1}10]_{B2}$ and $[110]_{B2}$, respectively. The lattice parameters are $a = a_0$, $b = c = \sqrt{2}a_0$, here a_0 is the lattice constants of cubic B2 phase. We focus on the orthorhombic B19 and monoclinic B19′ structures for the martensite phase observed experimentally in Ni–Ti–Cu and Ni–Ti–Zr shape memory alloys[11,12,16]. Figure 1 shows the supercell model of austenite and martensite phase of NiTi alloy. Geometry optimizations were implemented for all possible doping structures. More details of site preference for $Ti_{50}(Ni_{50-x}Cu_x)$ and $Ni_{50}(Ti_{50-x}Zr_x)$ alloys were shown in Supplementary Fig. S1, Supplementary Tables S1 and S2. The site occupation of B19 and B19′ phase corresponds to that of B2.

We calculate the most stable position of B2 phase with the principle of lowest energy first, and the site occupation of doped atoms of B19 and B19′ phase is set according to the B2. The energy difference between B2, B19

	B2				B19			B19′			
	Our calc.[15]	Exp.[42]	Other calc.[43,44]		Our calc.[15]	Other calc.[43,44]		Our calc.[15]	Exp.[45]	Other calc.[43,44]	
a(Å)	3.004	3.015	3.009	3.011	2.737	2.776	2.810	2.915	2.898	2.929	2.847
b(Å)	4.248	4.264	4.255	4.258	4.239	4.221	4.189	4.083	4.108	4.048	4.116
c(Å)	4.248	4.264	4.255	4.258	4.637	4.631	4.707	4.649	4.646	4.686	4.672
β(°)	90	90	90	90	90	90	90	98.26	98	97.8	97.78

Table 1. Lattice constants of B2, B19 and B19′ phases in NiTi (taken from our previous calculation ref[15]), compared with the experimental data and other ab initio calculations.

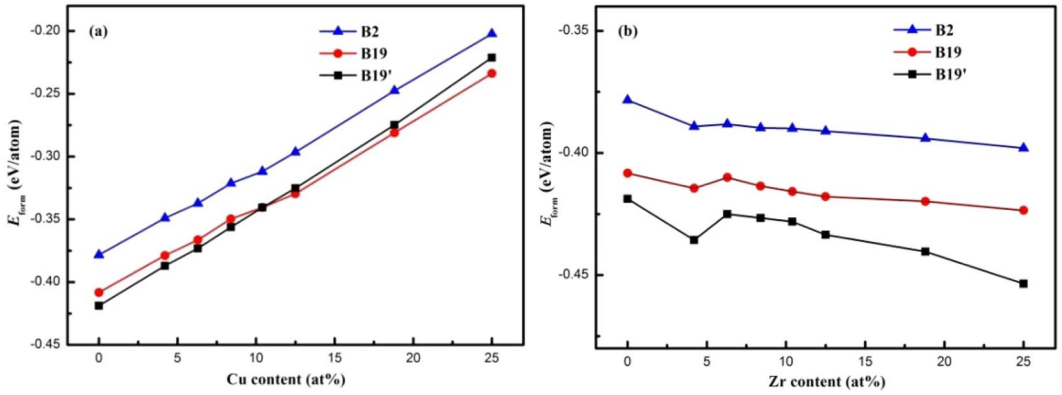

Figure 2. Formation energies, E_{form}, as a function of the addition content in quasi-equiatomic ternary (**a**) $Ti_{50}(Ni_{50-x}Cu_x)$ and (**b**) $Ni_{50}(Ti_{50-x}Zr_x)$ alloys. The trendline is a fit through all data points.

and B19′ phase is almost unaffected by the doping position. Moreover, the calculated deviations of energy of all possible doping position is about 0.2 eV.

The calculations are performed using DFT as implemented in the Vienna *Ab initio* Simulation Package[25–27] (VASP) together with plane-wave projector augmented wave[28] (PAW) pseudopotentials and the PW91[29] generalized gradient approximation[30] (GGA) for the exchange and correlation effects. The valence electron configurations for Ni, Ti, Cu and Zr are $3d^84s^2$, $3d^24s^2$, $3d^{10}4s^1$ and $4d^25s^1$, respectively. We tested k-point sampling[31] and an energy cutoff convergence for all supercells. As a result of the convergence tests, Brillouin zone sampling was performed using $4 \times 4 \times 4$ special k-point mesh, the plane-wave cutoff energy was set to 500 eV. In the calculations, the total energies were converged up to 10^{-4} eV/atom, and the atomic positions in our models were fully relaxed until the force of every atom was less than 0.01 eV/Å. We relaxed the structure with ISIF = 7 option (not change cell shape, change cell volume and not relax ions) first, and then, with ISIF = 2 option (not change cell shape, not change cell volume and relax ions) in VASP.

Structural parameters adopted in the present work are summarized in Table 1. The calculated lattice parameters are in line with each other and with the experimental result.

Results and Discussion

Effects of additions (Cu or Zr) on phase stability of ternary NiTi-based alloys. In order to analyze the effect of Cu or Zr additions on phase stability, we evaluate the formation energies (E_{form}) for B2, B19 and B19′ phases of $Ti_{50}(Ni_{50-x}Cu_x)$ and $Ni_{50}(Ti_{50-x}Zr_x)$ alloys, respectively. E_{form} is defined as the total energy of the alloy minus the concentration weighted average of the pure elements' total energies at their equilibrium volumes[32–34]. As previously mentioned, the $2 \times 2 \times 3$ supercell of B2, B19 and B19′ structures of $Ti_{50}(Ni_{50-x}Cu_x)$ and $Ni_{50}(Ti_{50-x}Zr_x)$ alloys that contains 48 atoms are constructed. It is calculated (per atom) as

$$E^1_{form} = \frac{E_{tot} - [24E\,(_{Ti}{}^{hcp}) + (24 - n)\,E\,(_{Ni}{}^{fcc}) + nE\,(_{Cu}{}^{fcc})]}{48} \quad (1)$$

$$E^2_{form} = \frac{E_{tot} - [24E\,(_{Ni}{}^{fcc}) + (24 - n)E\,(_{Ti}{}^{hcp}) + nE\,(_{Zr}{}^{hcp})]}{48} \quad (2)$$

where E^1_{form} and E^2_{form} are for $Ti_{50}Ni_{50-x}Cu_x$ and $Ni_{50}Ti_{50-x}Zr_x$ alloys respectively, E_{tot} is the total energy of $Ti_{50}Ni_{50-x}Cu_x$ and $Ni_{50}Ti_{50-x}Zr_x$ alloys, $E\,(_{Ni}{}^{fcc})$, $E\,(_{Ti}{}^{hcp})$, $E\,(_{Cu}{}^{fcc})$ and $E\,(_{Zr}{}^{hcp})$ denotes, respectively, the energy of one Ni, Ti, Cu and Zr atom in their bulk states, n is the number of doping atoms (Cu or Zr) in the supercell. The calculated results of E_{form} as a function of doping concentration are plotted in Fig. 2.

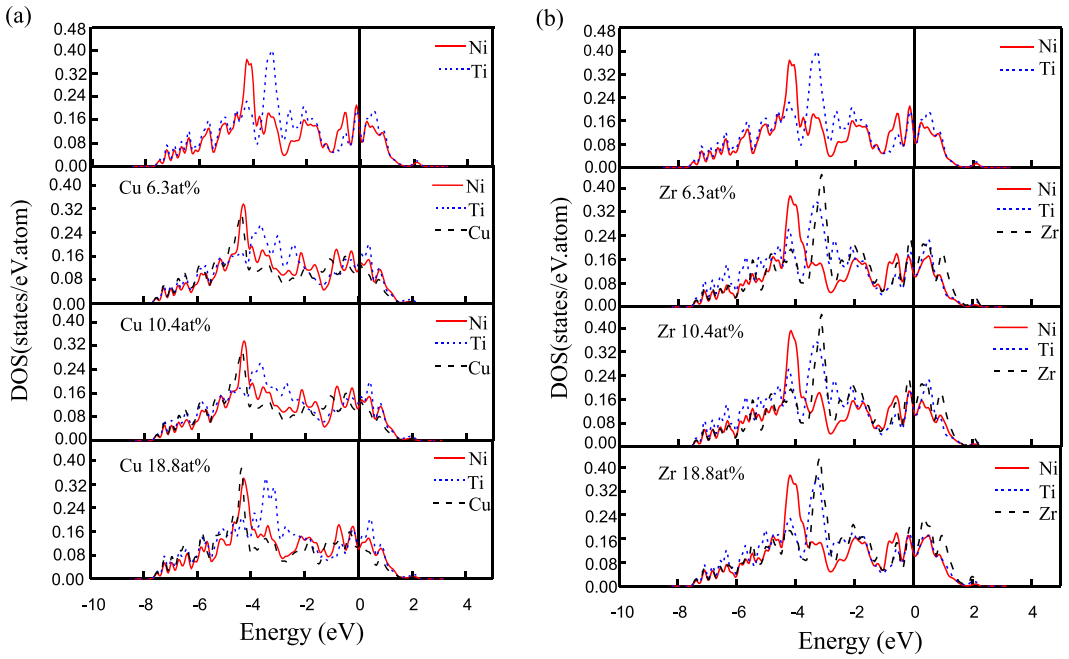

Figure 3. Partial density of states (PDOSs) of the doping atoms as well as their nearest Ti and Ni atoms in the austenitic phase of different doping concentration for (**a**) $Ti_{50}(Ni_{50-x}Cu_x)$ and (**b**) $Ni_{50}(Ti_{50-x}Zr_x)$ alloys. The vertical line denotes the Fermi level, which is located at 0 eV.

E_{form} of B2 phase is much higher than that of B19 and B19′ phases in NiTi alloy ($x = 0$), and, $E_{fB19'} < E_{fB19} < E_{fB2} < 0$, which reveals that the B19 and B19′ phases are more stable compared with the B2 phase, and, B19′ phase is the lowest temperature phase, which agrees with the experimental results[16].

The E_{form} of each phase increases almost linearly with the increasing of Cu content which indicates that the phase stabilities of three structurers become worse (see Fig. 2(a)). This is in accordance with the experimental results[17]. There is a crossover at the formation energy curve for Cu = 10.4 at.% concentration. For Cu < 10.4 at.%, the B19′ phase is more stable than B19 phase; for Cu > 10.4 at.%, the B19 phase is more stable than B19′ phase, which indicates the phase transition path changed. For Cu < 10.4 at.%, phase transition takes place from B2 → B19′, while for Cu ≥ 10.4 at.%, the MT path thus becomes B2 → B19. From the calculation of formation energies, the most stable martensitic phase was changed from monoclinic to orthorhombic (see Fig. 2(a)), which is also in accordance with previous experimental works[8,16].

For the Zr-doped, however, the formation energies of three phases decrease with the doping concentration, which means the stability for all phases increases with Zr doping. Moreover, the formation energy of B19′ is the lowest one. The B19′ phase is the most stable structure all the time with increasing x, which consistent with the previous results[11,12], see Fig. 2(b).

The partial density of states (PDOSs) of the austenitic phase with different doping concentration for $Ti_{50}(Ni_{50-x}Cu_x)$ and $Ni_{50}(Ti_{50-x}Zr_x)$ alloys have been calculated and plotted in Fig. 3. We can see that the PDOSs of Ni and Ti atoms have a sharp peak located at −4.4 and −3.5 eV, respectively, for pure NiTi alloy. The PDOSs of Cu atoms are similar to the Ni atoms, and, there is no obvious hybridization with the nearest neighbor Ti atoms. Cu doping weakens the overlap between Ti and Cu electronic states at −4 ~ −1.5 eV. With the increasing of the Cu concentration, the peak positions of Ti atoms and Ni-Cu resonated atoms shift to the higher energy slightly. This suggests that B2 phase become unstable with the increasing of Cu content, in accordance with the results of E_{form} (see Fig. 2(a)).

It can be seen from Fig. 3(b) that due to the Zr doping, the PDOSs of Zr atoms are similar to the Ti atoms, and there is obvious hybridization with the nearest neighbor Ti and Ni atoms. With the increase of Zr addition, there are the increasing resonant states between the Zr and its nearest neighbor Ti atoms at energy region −4 ~ −3 eV, which enhances the interaction between Ti and Zr atoms. The peak of Ni atoms and Ti-Zr resonated atoms shift to the lower energy slightly. This indicates that strong bonding states and thus increases the stability of the austenitic phase, which is in consistent with the formation energy result shown in Fig. 2(b).

Composition dependence of transformation temperature in $Ti_{50}(Ni_{50-x}Cu_x)$ and $Ni_{50}(Ti_{50-x}Zr_x)$ alloys. The transformation behaviors can be described by the energy differences (ΔE) between the austenitic B2 structure and martensitic B19 and B19′ structure, $\Delta E = E_{B2} - E_{B19/B19'}$. Table 2 summarizes the energy differences for all three phases in NiTi. The calculated results indicate that B19 phase is lower in energy than B2 by 29.95 meV/atom, and, the monoclinic B19′ phase is the lowest in energy ($\Delta E = E_{B2} - E_{B19'} = 40.39$ meV/atom) in NiTi alloys. The present calculations are in good accordance with other DFT studies.

The previous observation[32] shows that martensite transformation temperature is closely related to the value of ΔE, and, T_m usually increases with increasing ΔE. Figure 4 presents the concentration dependence of ΔE for the

ΔE	Present calc.	Other calc.[43]	Other calc.[44]
$E_{B2} - E_{B19}$	29.95	30.07	28.57
$E_{B2} - E_{B19'}$	40.39	41.91	39.46

Table 2. Computed energy differences $\Delta E = E_{B2} - E_{B19/B19'}$ (in meV/atom) in binary NiTi, compared with other first-principles studies.

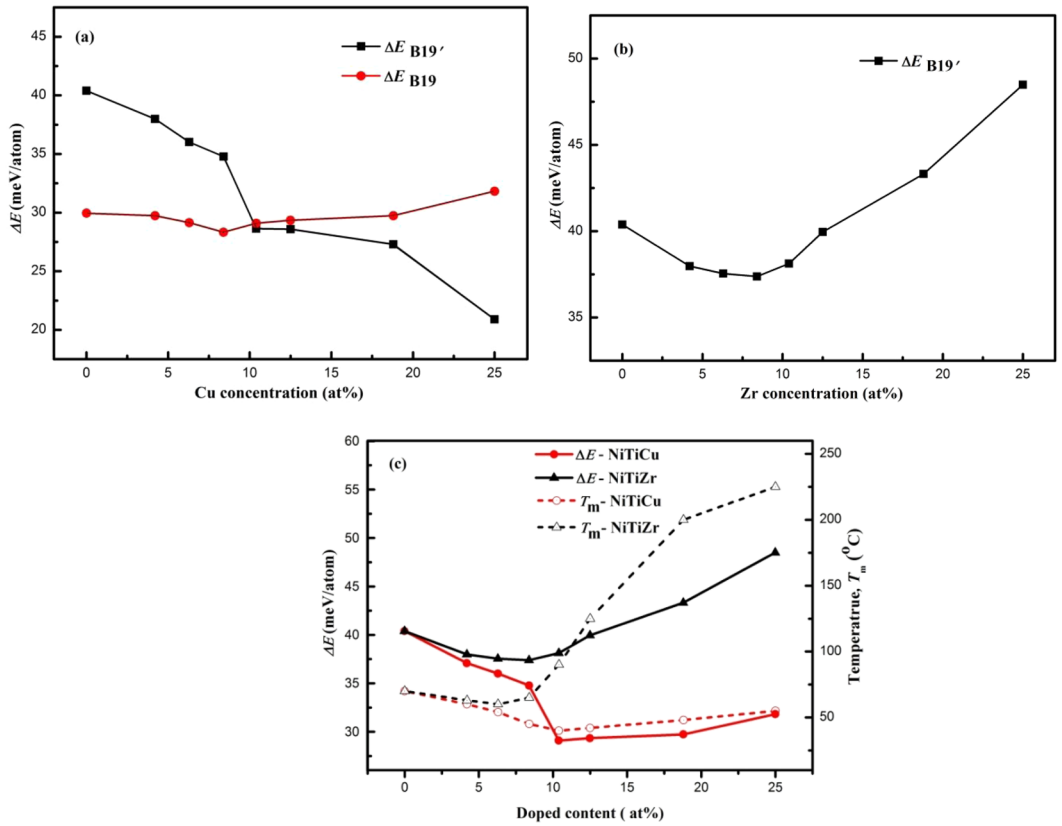

Figure 4. Dependency of the energy differences between austenite and martensite ΔE for (**a**) $Ti_{50}(Ni_{50-x}Cu_x)$ and (**b**) $Ni_{50}(Ti_{50-x}Zr_x)$ on doped content (0–25 at.%). (**c**) Composition dependence of ΔE and transformation temperature T_m of $Ti_{50}(Ni_{50-x}Cu_x)$ and $Ni_{50}(Ti_{50-x}Zr_x)$ alloys. The values of T_m refer to the right axis and those of ΔE to the left axis. T_m of Ni-Ti-Cu is cited from refs[16,35], T_m of Ni-Ti-Zr is cited from refs[10,13]. Lines are guides for the eyes.

$Ti_{50}(Ni_{50-x}Cu_x)$ and $Ni_{50}(Ti_{50-x}Zr_x)$ alloys. For $Ti_{50}(Ni_{50-x}Cu_x)$ alloys with low doping concentrations (Cu < 10.4 at.%), as $0 < \Delta E_{B19} < \Delta E_{B19'}$(see Fig. 4(a)), the most stable phase is B19′ phase. The $\Delta E_{B19'}$ decreases slightly with increasing x (see Fig. 4(a)), thus the lower energy is needed for the martensitic transformation. The lower ΔE corresponds to a lower T_m, therefore, the T_m decreases slightly. At high doping concentrations (Cu > 10.4 at.%), as $0 < \Delta E_{B19'} < \Delta E_{B19}$, the most stable phase is B19, and ΔE_{B19} increases slightly with increasing Cu content, thus a little higher T_m occurs.

It is clearly seen from Fig. 4(b) that, for Zr < 10.4 at.%, $\Delta E_{B19'}$ decreases slightly; with x further increasing, $\Delta E_{B19'}$ increases significantly. Lager ΔE indicates more energy is needed for the martensitic transformation thus corresponds to a higher T_m.

In Fig. 4(c), we plot the total energy differences between B2 and martensite phases (ΔE) as well as T_m as a function of the doping concentration of $Ti_{50}(Ni_{50-x}Cu_x)$ and $Ni_{50}(Ti_{50-x}Zr_x)$ systems. T_m of Ni–Ti–Cu is cited from refs[16,35], and T_m of Ni–Ti–Zr is cited from refs[10,13]. Addition of Cu decreases the T_m, and then increases slightly with further increasing of Cu content. This makes the T_m less sensitive to composition changes comparing with the binary NiTi alloys, which is in accordance with previous experimental works[8,9,16,17,35]. Zr addition raises the T_m obviously, which is fully in line with the experimental observations that the Zr additions increase the T_m dramatically[10,13].

Influence of Cu or Zr on the hysteresis. Hysteresis (ΔT) in shape memory alloys (SMAs) is the macroscopic presentation of the energy dissipation of the martensitic phase transformation, which plays an important role in their thermomechanical behavior. The geometric non-linear theory[36] of martensite specifies several

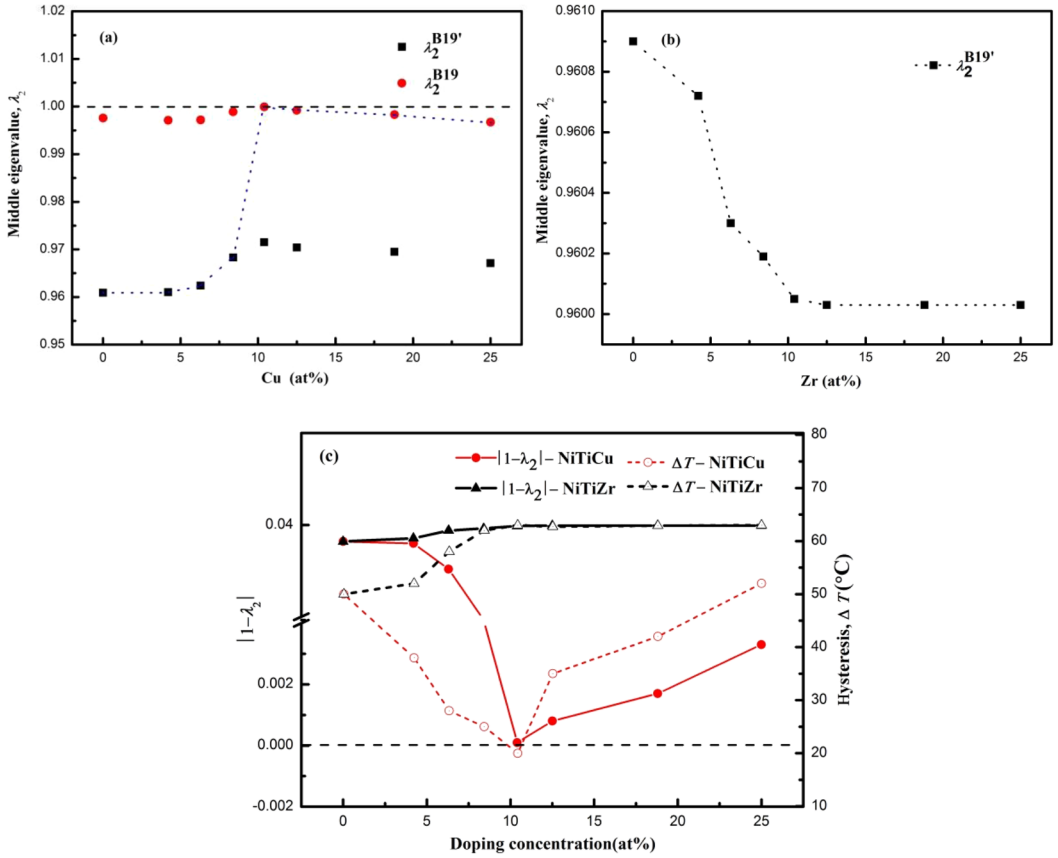

Figure 5. Middle eigenvalue λ_2 vs. doped concentration of (**a**) $Ti_{50}(Ni_{50-x}Cu_x)$ and (**b**) $Ni_{50}(Ti_{50-x}Zr_x)$ alloys. (**c**) Effect of addition content on the $|1-\lambda_2|$ and thermal hysteresis ΔT of $Ti_{50}(Ni_{50-x}Cu_x)$ and $Ni_{50}(Ti_{50-x}Zr_x)$ systems. The values of ΔT refer to the right axis and those of $|1-\lambda_2|$ to the left axis. ΔT of Ni-Ti-Cu is cited from refs[10,13,19,35,38,39]. ΔT of Ni-Ti-Zr is cited from refs[10,13].

conditions for SMAs with extremely low hysteresis. The first condition $\det(U) = \lambda_1\lambda_2\lambda_3 = 1$, represents no volume change during phase transformation, where U is the transformation stretch tensor that maps the martensite lattice to the austenite lattice, $\det U$ is its determinant and $\lambda_1 \le \lambda_2 \le \lambda_3$ are the ordered eigenvalues of U. The second condition $\lambda_2 = 1$ represents phase compatibility between austenite and martensite. The transformation stretch tensor between a bcc austenite and one particular lattice correspondence variant of an orthorhombic martensite is[37,38]

$$U = \begin{bmatrix} \beta & 0 & 0 \\ 0 & \dfrac{\alpha-\gamma}{2} & \dfrac{\alpha+\gamma}{2} \\ 0 & \dfrac{\alpha+\gamma}{2} & \dfrac{\alpha-\gamma}{2} \end{bmatrix}. \tag{3}$$

Their values are entirely determined by the lattice parameters of the austenite (a_0) and the orthorhombic martensite phase (a, b, c): $\beta = \lambda_1 = \frac{a}{a_0}$, $\alpha = \lambda_2 = \frac{b}{\sqrt{2}\,a_0}$, $\gamma = \lambda_3 = \frac{c}{\sqrt{2}\,a_0}$.

According to the above theory, Cui *et al.*[38] discovered that there is a strong relationship between hysteresis (ΔT) and λ_2, but not with det(U), in Ni–Ti–Cu and Ni–Ti–Pd thin-films. Zhang *et al.*[39] further demonstrated the same correlation for bulk alloys of Ni–Ti–Au, Ni–Ti–Cu, Ni–Ti–Pd, and Ni–Ti–Pt. Low hysteresis with phase compatibility between austenite and martensite was investigated in $Ti_{50}(Ni_{50-x}Pd_x)$ system[37]. Recently, the direct correlation between thermal hysteresis and functional stability was demonstrated in binary (Ni-Ti), ternary (Ni-Ti-Cu, Ni-Ti-Pd) and quaternary (Ni-Ti-Cu-Pd) SMAs[40,41].

To investigate the influence of alloy elements content on thermal hysteresis (ΔT) in the $Ti_{50}(Ni_{50-x}Cu_x)$ and $Ni_{50}(Ti_{50-x}Zr_x)$ systems, we calculated λ_2 values by $\lambda_2^{B19} = b_{B19}/b_{B2}$ for B2 → B19 crystallographic transformation, λ_2 shown as $\lambda_2^{B19'} = b_{B19'}\sin\beta/b_{B2}$ for B2 → B19′ phase transformation, where b_{B2}, b_{B19} and $b_{B19'}$ are the lattice parameters of the B2, B19 and B19′ structures in the [010] direction, respectively, and β is the monoclinic angle of the crystal structure of B19′ martensite. The calculated structural parameters of $Ti_{50}(Ni_{50-x}Cu_x)$ and $Ni_{50}(Ti_{50-x}Zr_x)$ for different doping concentration are listed in Supplementary Tables S3 and S4. The variations of λ_2 vs. doping concentration for these alloys were shown in Fig. 5.

As indicated in Fig. 5(a), an increase in the percentage of Cu (substituted for Ni) increases the value of λ_2, further approaching 1; for Cu content at 10.4 at.%, $\lambda_2 = 1$; Cu > 10.4 at.%, λ_2 is far from 1. In Fig. 5(c), $|1 - \lambda_2|$ was calculated in the present study while the corresponding ΔT values were taken from the literature[10,13,19,35,38,39]. One can see a remarkable collapse of the data onto two lines shaped like a V for $Ti_{50}(Ni_{50-x}Cu_x)$, and the widths of the thermal hysteresis have a minimum for $|1 - \lambda_2|$ approaches 0 (Cu = 10.4 at.%). λ_2 quantifies the geometric compatibility of the martensite and the austenite, and the fit between the two phases increases as λ_2 approaches 1[37–41]. The most stable martensite phase was changed from monoclinic to orthorhombic structure for $Ti_{50}(Ni_{50-x}Cu_x)$ alloys, which increases the phase compatibility, making λ_2 approach 1. For other λ_2 value which is lower or higher than 1, wider thermal hysteresis is observed. Adding Cu lower the width of the thermal hysteresis, ΔT appears to be minimized when Cu content at about 10.4 at.%at.%.

The value of λ_2 decrease slightly for Zr < 10.4 at.%, and then nearly stable, keeping further from 1 (see Fig. 5(b)). This is because phase compatibility is reduced. With increasing of Zr content, λ_2 deviates from 1 leading higher thermal hysteresis temperature for martensitic transformation. Therefore, replacement of Ti by Zr in the NiTi alloy raises the ΔT slightly in $Ni_{50}(Ti_{50-x}Zr_x)$ SMAs, which are in line with other literatures[10,13].

Conclusions

Our first-principles calculations on formation energies E_{form}, energy differences between austenite and martensite ΔE and the middle eigenvalue of transformation stretch tensor λ_2 for $Ti_{50}(Ni_{50-x}Cu_x)$ and $Ni_{50}(Ti_{50-x}Zr_x)$ systems allow us to draw the following conclusions. For $Ti_{50}(Ni_{50-x}Cu_x)$ alloys, when the doping Cu concentrations are less than 10.4 at.%, phase transformation takes place from B2 to monoclinic B19′ phase, while the doping concentration ≥10.4 at.%, phase transformation happens from B2 to orthorhombic B19 phase. According to the results of ΔE and λ_2, for Cu < 10.4 at.%, adding Cu slightly decreases T_m and thermal hysteresis ΔT, moreover, gets a minimum of the widths of thermal hysteresis; with further doping, T_m and ΔT increase slightly. In short, the addition of Cu results in a decrease of T_m and ΔT. The present investigation exhibits that the replacement of Ti by Zr rises transformation temperature significantly, and increase the hysteresis slightly. $Ni_{50}(Ti_{50-x}Zr_x)$ alloy remains the B19′ martensitic phase, which leads the phase compatibility between austenite and martensite reduced and larger lattice deformation involved.

Data Availability

The data that support the findings of this study are available from the corresponding authors upon reasonable request.

References

1. Chakravarty, S., Kee, H. Y. & Volker, K. An explanation for a universality of transition temperatures in families of copper oxide superconductors. *Nature* **428**, 53–55 (2004).
2. Buehler, W. J. & Wiley, R. C. TiNi-ductile intermetallic compound. *ASM-Trans* **55**, 269–276 (1962).
3. Firstov, G., Van Humbeeck, J. & Koval, Y. N. High-temperature shape memory alloys: some recent developments. *Mater. Sci. Eng. A* **378**, 2–10 (2004).
4. Bozzolo, G., Noebe, R. D. & Mosca, H. O. Site preference of ternary alloying additions to NiTi: Fe, Pt, Pd, Au, Al, Cu, Zr and Hf. *J. Alloys Compd.* **389**, 80–94 (2005).
5. Zhou, Y. *et al*. Strain glass in doped $Ti_{50}(Ni_{50-x}D_x)$(D = Co, Cr, Mn) alloys: Implication for the generality of strain glass in defect-containing ferroelastic systems. *Acta Mater.* **58**, 5433–5442 (2010).
6. Wang, X., Shang, J. X., Wang, F. H. & Chen, Y. Origin of the strain glass transition in $Ti_{50}(Ni_{50-x}D_x)$ alloys. *J. Alloys Compd.* **678**, 325–328 (2016).
7. Wang, D. *et al*. Strain glass in Fe-doped Ti–Ni. *Acta Mater.* **58**, 6206–6215 (2010).
8. Nam, T. H., Saburi, T., Nakata, Y. & Shimizu, Ki Shape memory characteristics and lattice deformation in Ti–Ni–Cu alloys. *Mater. Trans., JIM* **31**, 1050–1056 (1990).
9. Mercier, O. & Melton, K. N. The substitution of Cu for Ni in NiTi shape memory alloys. *Metall. Trans. A* **10**, 387 (1979).
10. Ma, J., Karaman, I. & Noebe, R. D. High temperature shape memory alloys. *Int. Mater. Rev.* **55**, 257–315 (2010).
11. Meisner, L. L., Sivokha, V. P. & Perevalova, O. B. Formation features of fine structure of the $Ni_{50}Ti_{40}Zr_{10}$ alloy under different thermal treatment. *Physica B* **262**, 49–54 (1999).
12. Meisner, L. & Sivokha, V. Deformation of Crystal Lattice in the Process of Martensitic Transformation in Alloys of $Ni_{50}Ti_{50-x}Zr_x$. *J. Phys. IV* **05**, 765–769 (1995).
13. Inoue, S., Sawada, N. & Namazu, T. Effect of Zr content on mechanical properties of Ti–Ni–Zr shape memory alloy films prepared by dc magnetron sputtering. *Vacuum* **83**, 664–667 (2009).
14. Hu, Q. M. *et al*. Effect of Zr on the properties of (TiZr)Ni alloys from first-principles calculations. *Phys. Rev. B* **76**, 224201 (2007).
15. Ma, L., Wang, X. & Shang, J. X. Effect of Pd in NiTi on the martensitic transformation temperatures and hysteresis: a first-principles study. *Acta Phys. Sin.* **63**, 233103 (2014).
16. Otsuka, K. & Ren, X. Recent developments in the research of shape memory alloys. *Intermetallics* **7**, 511–528 (1999).
17. Otsuka, K. & Ren, X. Physical metallurgy of Ti–Ni-based shape memory alloys. *Prog. Mater Sci.* **50**, 511–678 (2005).
18. Feng, Z. W., Gao, B. D., Wang, J. B., Qian, D. F. & Liu, Y. X. Influence of Zr additions on shape-memory effect and mechanical properties of Ni-rich NiTi alloys. *Mater. Sci. Forum* **394–395**, 365–368 (2002).
19. Frenzel, J. *et al*. On the effect of alloy composition on martensite start temperatures and latent heats in Ni–Ti-based shape memory alloys. *Acta Mater.* **90**, 213–231 (2015).
20. Zarinejad, M. & Liu, Y. Dependence of transformation temperatures of NiTi-based shape-memory alloys on the number and concentration of valence electrons. *Adv. Funct. Mater.* **18**, 2789–2794 (2008).
21. Singh, N. *et al*. Effect of ternary additions to structural properties of NiTi alloys. *Comput. Mater. Sci.* **112**, 347–355 (2016).
22. Gou, L., Liu, Y. & Ng, T. Y. An investigation on the crystal structures of $Ti_{50}Ni_{50-x}Cu_x$ shape memory alloys based on density functional theory calculations. *Intermetallics* **53**, 20–25 (2014).
23. Lu, J. M., Hu, Q. M. & Yang, R. Composition-dependent elastic properties and electronic structures of off-stoichiometric TiNi from first-principles calculations. *Acta Mater.* **56**, 4913–4920 (2008).
24. Chluba, C. *et al*. Ultralow-fatigue shape memory alloy films. *Science* **348**, 1004–1007 (2015).
25. Kresse, G. & Hafner, J. Ab initio molecular dynamics for open-shell transition metals. *Phys. Rev. B* **48**, 13115–13118 (1993).
26. Kresse, G. & Furthmüller, J. Efficient iterative schemes for ab initio total-energy calculations using a plane-wave basis set. *Phys. Rev. B* **54**, 11169–11186 (1996).

27. Kresse, G. & Furthmüller, J. Efficiency of ab-initio total energy calculations for metals and semiconductors using a plane-wave basis set. *Comput. Mater. Sci.* **6**, 15–50 (1996).
28. Kresse, G. & Joubert, D. From ultrasoft pseudopotentials to the projector augmented-wave method. *Phys. Rev. B* **59**, 1758–1775 (1999).
29. Perdew, J. P. *et al.* Atoms, molecules, solids, and surfaces: Applications of the generalized gradient approximation for exchange and correlation. *Phys. Rev. B* **46**, 6671–6687 (1992).
30. Perdew, J. P. & Wang, Y. Accurate and simple analytic representation of the electron-gas correlation energy. *Phys. Rev. B* **45**, 13244–13249 (1992).
31. Monkhorst, H. J. & Pack, J. D. Special points for Brillouin-zone integrations. *Phys. Rev. B* **13**, 5188–5192 (1976).
32. Chen, J., Li, Y., Shang, J. & Xu, H. First principles calculations on martensitic transformation and phase instability of Ni–Mn–Ga high temperature shape memory alloys. *Appl. Phys. Lett.* **89**, 231921 (2006).
33. Alonso, P. & Rubiolo, G. Relative stability of bcc structures in ternary alloys with $Ti_{50}Al_{25}Mo_{25}$ composition. *Phys. Rev. B* **62**, 237–242 (2000).
34. Holec, D., Friák, M., Dlouhý, A. & Neugebauer, J. Ab initio study of point defects in NiTi-based alloys. *Phys. Rev. B* **89**, 014110 (2014).
35. Zarnetta, R., Buenconsejo, P. J. S., Savan, A., Thienhaus, S. & Ludwig, A. High-throughput study of martensitic transformations in the complete Ti–Ni–Cu system. *Intermetallics* **26**, 98–109 (2012).
36. Ball, J. M. & James, R. D. Proposed experimental tests of a theory of fine microstructure and the two-well problem. *Philos. Trans. R. Soc. London. A* **338**, 389–450 (1992).
37. Delville, R. *et al.* Transmission electron microscopy study of phase compatibility in low hysteresis shape memory alloys. *Philos. Mag.* **90**, 177–195 (2010).
38. Cui, J. *et al.* Combinatorial search of thermoelastic shape-memory alloys with extremely small hysteresis width. *Nat. Mater.* **5**, 286–290 (2006).
39. Zhang, Z., James, R. D. & Müller, S. Energy barriers and hysteresis in martensitic phase transformations. *Acta Mater.* **57**, 4332–4352 (2009).
40. Zarnetta, R. *et al.* Identification of quaternary shape memory alloys with near-zero thermal hysteresis and unprecedented functional stability. *Adv. Funct. Mater.* **20**, 1917–1923 (2010).
41. Koenig, D., Zarnetta, R., Savan, A., Brunken, H. & Ludwig, A. Phase transformation, structural and functional fatigue properties of Ti–Ni–Hf shape memory thin film. *Acta Mater.* **59**, 3267–3275 (2011).
42. Philip, T. & Beck, P. A. CsCl-type ordered structures in binary alloys of transition elements. *Trans AIME J Metals* **209**, 1269–1271 (1957).
43. Huang, X., Ackland, G. J. & Rabe, K. M. Crystal structures and shape-memory behaviour of NiTi. *Nat. Mater.* **2**, 307–311 (2003).
44. Kibey, S., Sehitoglu, H. & Johnson, D. Energy landscape for martensitic phase transformation in shape memory NiTi. *Acta Mater.* **57**, 1624–1629 (2009).
45. Kudoh, Y., Tokonami, M., Miyazaki, S. & Otsuka, K. Crystal-structure of the martensite in Ti-49.2at%Ni alloy analyzed by the single-crystal X-ray-diffration method. *Acta Metall.* **33**, 2049–2056 (1985).

Acknowledgements

The present work was financially supported by the National Natural Science Foundation of China (Grant No. 51371017), and the Natural Science Foundation of Technology Department (QKHLH [2015]7021).

Author Contributions

X.Y. and J.S. were responsible for the study design. X.Y. and L.M. made substantial contributions to the acquisition, analysis, or interpretation of data for the work. X.Y. and J.S. drafted the work or revised it critically for important intellectual content. All authors read and approved the final manuscript.

Additional Information

Supplementary information accompanies this paper at https://doi.org/10.1038/s41598-019-40100-z.

Competing Interests: The authors declare no competing interests.

Publisher's note: Springer Nature remains neutral with regard to jurisdictional claims in published maps and institutional affiliations.